International Journal of Latest Engineering Research and Applications (IJLERA) ISSN: 2455-7137

Volume – 07, Issue – 11, November 2022, PP – 68-78

Assessment of heat transfer mechanism in Jeffrey nanoliquid stagnation-point flow along a convectively heated expanding device featuring nonlinear thermal radiation

O. O. Akanbi[1], E. O. Fatunmbi[2]

[1-2]*Department of Mathematics and Statistics, Federal Polytechnic, Ilaro, Nigeria*

Abstract: The investigation communicated in this study features the mechanism of heat distribution in stagnation-point flow of hydromagnetic Jeffery fluid conveying tiny nanoparticles along a porous expanding sheet. The formulated mathematical model is made of two dimensional permeable sheet which is convectively heated alongside the impacts of nonlinear thermal radiation together with ex ternal magnetic field. The transformation of the model equations from partial to ordinary derivatives is actualized by similarity techniques and thereafter a numerical approach via shooting procedures accompanied with Runge-Kutta-Fehlberg scheme is applied to provide solutions to the transmuted equations. Efforts were made to scrutinize the impacts of the emerging physical quantities on the non-dimensional factors, skin frictional factor as well as heat transfer mechanism via various graphs. A strong positive correlation occurs in the results obtained in the present results and existing data in literature in the limiting condition. The outcomes of the analysis indicate a depletion of temperature profiles for higher Deborah number whereas the thermal field escalates with magnetic field, surface convection and thermal radiation terms. Heat transfer mechanism across the surface dimin ishes with thermophoretic and brownian motion terms but stretching parameter, surface convection term and Prandtl number boost the heat transfer.

Keywords: Heat transfer; Jeffrey nanoliquid; nonlinear thermal radiation; stagnation-point flow

1. Introduction

Investigations conducted on the boundary layer flows generated by expanding sheet provide an extensive engineering and industrial applications. These applications are common in extrusion activities; plastic sheet and metal, electronic chips, crystal growing, cooling of metallic sheet, glass blowing, etc. (Anderson, 2002; Kumar, 2009; Fatunmbi & Adeniyan, 2018). The pioneering work on such phenomenon was attributed to Crane (1970) who designed such a problem in a two-dimensional horizontally expanding surface whose velocity and distance from a fixed position have direct proportion. In furtherance to such work, a good number of researchers have deliberated on such a concept by introducing various assumptions, configurations and parameters of interest. For instance, a report detailing the transport of a reactive Jeffrey fluid configured in a sheet which expands linearly with radiation effects was deliberated by Mishra (2017) while Pal et al. (2019) included the effects of viscous dissipation, Ohmic heating and entropy analysis to improve on the work of Mishra (2017). Jena et al. (2016) evaluated heat-mass propagation in hydromagnetic Jeffrey fluid when heat source/sink together with boundary temperature and concentration exponent are incorporated where as Fatunmbi and Okoya (2020) recently conducted such an analysis with emphasis on heat flow over a non-linearly stretched sheet using the micropolar fluid being influenced by thermal radiation.

Owing to numerous applications being derived from the studies related to the non-Newtonian fluids various scientists and researchers have developed more interest on such analysis. Regularly, such real applications are encountered in engineering, technology and manufacturing operations including food sciences, chemical, mechanical and biomedical processes, textiles manufacturing, oil drilling, biological fluids, etc. Besides, the inappropriateness of the Navier-Stokes model to capture the intrinsic properties of these widely used industrial and engineering complex fluids has boosted the investigations of such fluids Mabood & Das (2019). Classification of the non-Newtonian fluids includes viscoelastic, time-dependent and time-independent types. However, there are complex and complicated fluids which manifest the properties that are common to these categories and at such, no single constitutive equation can adequately contain the characteristics features of the non-Newtonian fluids models due to differences in rheological properties. Hence, diverse models exist such as the Jeffrey fluids, Johnson-Segalman fluid, micropolar fluids, Williamson fluids, Giesekus fluids, Casson fluids and so on. These models have been derived to depict the non-Newtonian fluids motion under different conditions and rheology Dalir et al. (2015). One of the common non-Newtonian fluids is the Jeffrey fluid, it manifests the viscoelastic properties and characterizes relaxation and retardation times behaviour.

Common applications of this kind of fluids can be encountered in polymer processes as well as in bio-fluids, such applications have aroused the interest of many researchers (Zeeshan & Majeed; Hayat et al., 2012; Kazim et al., 2019) to examine the fluids on various configurations and assumptions. A new class of highly conducting fluid which provides better heat transfer characteristics with improved thermal conduction in comparison to the usual traditional fluid like water, oil, ethylene glycol, etc. is referred to as nanofluid, Choi & Eastman (1995). This category of fluids contains of minute particles called nanoparticles which are made up of metals, oxides, etc. suspended in the liquid. This fluid is applicable in most most engineering and industrial operations like atomic reactors, drug manufacturing, transportation systems, electronic cooling of components, etc.(Mabood et al., 2019; Prasannakumara et al. 2017; Ibrahim & Gamachu, 2019).

When fluid flow impinges on a solid object at a point, the fluid velocity at that point becomes zero and the pressure, heat transfer as well as mass deposition attain highest level at that region. Such a point is referred to as the stagnation point and was initially investigated by Hiemenz (1911) on a two-dimensional horizontal plate. The author employed similarity quantities techniques to modify the formulated equations into ordinary derivatives. Such a phenomenon finds considerable applications in engineering and technological works which includes extrusion of polymers in meltspinning processes, the cooling of electronic gadgets by fans, the continuous casting of metals, to mention a few (Batool & Ashraf, 2013; Ishak et al., 2009). In respect of these crucial applications derivable from such a subject, many researchers have devoted time and energy to investigate it under different assumptions and different geometries. A lot of research works have been done in this regard, few of such investigations can be found in Bhattacharyya (2013); Iqbal et al. (2017); Ibrahim et al. (2013). The inclusion of thermal radiation in the heat transport field is significant in the aspect of engineering and manufacturing activities operating with high temperature. In such activities like hot rolling, electrical power generation, solar power technology, nuclear reactors and so on, it is crucial to consider thermal radiation effect for the purpose of developing energy conversion systems. Generally, the use of linear thermal radiation can only be effective in situations of low temperature distribution in the flow region. However, in case of high thermal distribution in the flow field, nonlinear thermal radiation becomes effective as reported by Mabood et al. (2016); Lakshmi et al. (2019) and Gbadeyan et al. (2020).

Inspired by the above analysis, the purpose of this research is to numerically examine transport model of nonlinear radiative hydromagnetic Jeffrey fluid which contains tiny nanoparticles towards a stagnation-point. The fluid motion being designed over a porous elongated sheet with essential parameters of interest like thermophoresis, Brownian motion, viscous and Darcy dissipation coupled with convective heat transport at the wall. These parameters feature in the current model due to their relevance and real applications in various engineering and industrial activities.

2. Design and Problem Development

For the development of the problem and governing equations relevant to the current study, it is assumed that the fluid motion is two-dimensional, time-independent and incompressible over a permeable expanding plate in the neighbourhood of stagnation point. The working fluid is the Jeffrey fluid consisting of tiny nanoparticles featuring thermophoresis influence and brownian motion effect. The steady state flow is bounded by (x, y) axes as the transport coordinate system. In this view, the fluid transport is routed in the path of x axis but y axis is perpendicular to the leading edge while the constant magnetic field is imposed parallel to y direction as portrayed in figure 1. The model ignores induced magnetic field influence by assuming a small magnetic Reynolds number, variable fluid properties are not considered, chemical reaction effect is not taken into consideration, the sheet also features the imposition of two opposing but equivalent forces along the stretched surface with a fixed origin stationed at point $y = 0$ whereas the Jeffrey nanoliquid permeates through the region $y \geq 0$. The stretching plate temperature is convectively heated by a hot fluid characterized by temperature T_f. In the thermal region, the existence of nonlinear thermal radiation, fluid dissipating, Ohmic heating as well as Darcy heating effects are captured.

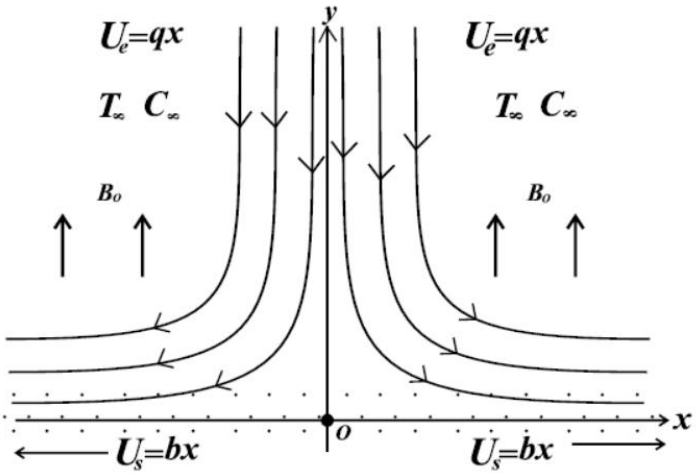

Fig. 1 Flow configuration

2.1 Equations governing the problem

Holding tight to the aforementioned assumptions together with with boundary layer approximation, the relevant governing equations have been developed and stated in Eqs. (1-4) (see SDalir et al., 2015; Fatunmbi & Adeniyan, 2020).

$$\frac{\partial v}{\partial y} = -\frac{\partial u}{\partial x}, \tag{1}$$

$$v\frac{\partial u}{\partial y} + u\frac{\partial u}{\partial x} - u_\infty \frac{du_\infty}{dx} = \frac{\mu}{\rho(1+\alpha)}\left[\frac{\partial^2 u}{\partial y^2} + \lambda\left(u\frac{\partial^3 u}{\partial x \partial y^2} - \frac{\partial u}{\partial x}\frac{\partial^2 u}{\partial y^2} + \frac{\partial u}{\partial y}\frac{\partial^2 u}{\partial x \partial y} + \nu\frac{\partial^3 u}{\partial y^3}\right)\right] - \left(\frac{\sigma B_0^2}{\rho} + \frac{\mu}{\rho k_p}\right)(u - u_\infty), \tag{2}$$

$$v\frac{\partial T}{\partial y} + u\frac{\partial T}{\partial x} = \frac{k}{\rho c_p}\frac{\partial^2 T}{\partial y^2} + \tau\left[\frac{D_T}{T_\infty}\left(\frac{\partial T}{\partial y}\right)^2 + D_B\left(\frac{\partial T}{\partial y}\frac{\partial C}{\partial y}\right)\right] + \left(\frac{\sigma B_0^2}{\rho c_p} + \frac{\mu}{\rho c_p k_p}\right)(u - u_\infty)^2 + \frac{\nu}{c_p}\left(\frac{\partial u}{\partial y}\right)^2 + \frac{16\sigma^\star}{3k_\star \rho c_p}\left(T^3\frac{\partial^2 T}{\partial y^2} + 3T^2\left(\frac{\partial T}{\partial y}\right)^2\right), \tag{3}$$

$$v\frac{\partial C}{\partial y} + u\frac{\partial C}{\partial x} = D_B\frac{\partial C^2}{\partial y^2} + \frac{D_T}{T_\infty}\left(\frac{\partial^2 T}{\partial y^2}\right). \tag{4}$$

Associated with equations (1-4) are the underlisted boundary constrains:

$$\begin{aligned} &At\ y = 0 : v = v_w, -k\frac{\partial T}{\partial y} = h_T\left(T_f - T\right), C = C_w, u = u_w = ax, \\ &\text{as } y \to \infty : \ \frac{\partial u}{\partial y} \to 0, T \to T_\infty, C \to C_\infty, u \to u_\infty = cx. \end{aligned} \tag{5}$$

The included symbols in equations (1-5) are: u, v denoting velocities in x, y direction while λ, $T(T_\infty)$, $C(C_\infty)$, ν, ρ, μ, $u_w(u_\infty)$ and σ sequentially indicates relaxation time, temperature(free stream temperature), concentration(free stream concentration of nanoparticles), kinematic viscosity, den sity, dynamic viscosity, wall(free stream) velocity and electrical conductivity. Further, $(\rho c_p)_f$, D_T, k, D_B,

K^*, k^*, σ^*, h_T , K_r and describes heat capacity of the fluid, thermophoretic coefficient, thermal con ductivity, Brownian coefficient, porous medium permeability, mean absorption coefficient, Stefan Boltzmann constant, heat transfer coefficient, chemical reaction rate whereas α denotes relaxation time ratio retardation time.

The under listed similarity quantities (6) are used to further transmute the transport equations from partial into ordinary derivatives. Hence, in view of (6), equation (1) is fulfilled while equations (7-9) are the ordinary derivatives derived from the governing equations (2-5) whereas equation (10) depicts the transformed boundary conditions.

$$\begin{aligned}&\phi(\eta)\left(C_w-C_\infty\right)=\left(C-C_\infty\right), \frac{\eta}{y}=\sqrt{\frac{a}{\nu}}, \theta(\eta)\left(T_f-T_\infty\right)=\left(T-T_\infty\right)\\&u=ax\frac{df}{d\eta},\ v=\sqrt{a\nu}f(\eta).\end{aligned} \tag{6}$$

$$\frac{d^3f}{d\eta^3}+(1+\alpha)\left(f(\eta)\frac{d^2f}{d\eta^2}-\left(\frac{df}{d\eta}\right)^2\right)+\delta\left(\left(\frac{d^2f}{d\eta^2}\right)^2-f(\eta)\frac{d^4f}{d\eta^4}\right)+(1+\alpha)H^2-(1+\alpha)\left[M+Da\right]\left(\frac{df}{d\eta}-H\right)=0, \tag{7}$$

$$\begin{aligned}&\left(1+R\left(1+(Tr-1)\theta(\eta)\right)^3\right)\frac{d^2\theta}{d\eta^2}+3R\left(Tr-1\right)\left(\frac{df}{d\eta}\right)^2\left(1+(Tr-1)\theta(\eta)\right)^2+PrEc(M+Da)\\&\left(\frac{df}{d\eta}-H\right)^2+Pr\left[f(\eta)\frac{d\theta}{d\eta}+Ec\left(\frac{d^2f}{d\eta^2}\right)^2+Nt\left(\frac{d\theta}{d\eta}\right)^2+Nb\frac{d\theta}{d\eta}\frac{d\phi}{d\eta}+MEc\left(\frac{d\theta}{d\eta}\right)^2\right]=0,\end{aligned} \tag{8}$$

$$\frac{d^2\phi}{d\eta^2}+\frac{Nt}{Nb}\frac{d^2\theta}{d\eta^2}+Scf\frac{d\phi}{d\eta}=0, \tag{9}$$

Likewise, the wall conditions simply transform to:

$$\begin{aligned}&At\ \eta=0:\frac{df}{d\eta}=1,\phi(\eta)=1,f(\eta)=fw,\frac{d\theta}{d\eta}=-\xi\left(1-\theta(\eta)\right),\\&As\ \eta\to0:\frac{df}{d\eta}=H,\frac{d^2f}{d\eta^2}=0,\phi(\eta)\to0,\theta(\eta)\to0.\end{aligned} \tag{10}$$

In the ordinary derivatives (7-10), differentiation is done with respect to η whereas ξ (surface convection term), *fw* (suction/injection term), *Ec* (Eckert number), *T r* (temperature ratio), δ (Deborah number), *M* (Magnetic field term), *Sc* (Schmidt number), *H* (Velocity ratio parameter), *R* (Radiation term), *N t* (Thermophoresis parameter), *P r* (Prandtl number) and *N b* (Brownian motion) are orderly described as follows:

$$\begin{aligned}&\xi=\frac{h_T}{k}\sqrt{\frac{\nu}{a}},fw=-\frac{v_w}{\sqrt{a\nu}},Ec=\frac{u_w^2}{c_p(T_f-T_\infty)},Tr=\frac{T_f}{T_\infty},\delta=a\lambda,M=\frac{\sigma B_0^2}{a\rho},Sc=\frac{\nu}{D_B}\\&H=\frac{c}{a},R=\frac{16T_\infty^3\sigma^\star}{3k^\star k},Nt=\tau\frac{D_T\left(T_f-T_\infty\right)}{T_\infty\nu},Pr=\frac{\mu c_p}{k},Nb=\tau\frac{D_B\left(C_w-C_\infty\right)}{\nu_\infty}.\end{aligned} \tag{11}$$

Moreover, the appropriate quantities of interest in the ongoing analysis are described as the Nusselt number Nu_x and skin friction coefficient C_{fx} as stated orderly in equation (12).

$$Nu_x=\frac{xh_w}{k\left(T_w-T_\infty\right)},C_{fx}=\frac{S_w}{\rho u_w^2}. \tag{12}$$

The dimensionless components of these quantities are

$$Nu_x=-\left[1+R\left(1+(Tr-1)\theta(\eta)\right)^3\right]Re_x^{1/2}\frac{d\theta}{d\eta}\ at\ \eta=0, \tag{13}$$

$$C_{fx}=\frac{1}{Re_x^{1/2}(1+\alpha)}\left[\frac{d^2f}{d\eta^2}+\delta\left[\frac{df}{d\eta}\frac{d^2f}{d\eta^2}-f(\eta)\frac{d^3f}{d\eta^3}\right]\right]\ at\ \eta=0, \tag{14}$$

where $S_w=\frac{\mu}{1+\alpha}\left[\left(\frac{\partial u}{\partial y}\right)+\lambda\left(u\frac{\partial^2u}{\partial x\partial y}+v\frac{\partial^2u}{\partial y^2}\right)\right]_{y=0}$ indicates shear stress and $h_w=-\left[\left(k+\frac{16T^3\sigma}{3k^\star}\right)\frac{\partial T}{\partial y}\right]_{y=0}$ connotes surface heat flux.

3. Solution method and results validation

The governing equations resulted from the problem under study are highly nonlinear. It is against this backdrop that a numerical means has been adopted by the use of shooting technique accom panied by Runge-Kutta-Fehlberg integration scheme is employed to obtain the needed solution to the equations. The technique used here has been elucidated by quite a number of researchers in the literature as simple, suitable and stable. For details of the numerical method, readers can check Mabood *et al.* [53], Fatunmbi and Okoya (2020), following previous authors, the parameters values for the computations in this study are $H = R = fw$, $Ec = 0.1$, $\alpha = 0.3 = \delta$, $N\,b = 0.5$, $Da = 0.2$, $N\,t = 0.5$, $P\,r = 0.72$, $Sc = 0.6$, $T\,r = 1.2$. The correctness of the results gotten in the current work is established by comparing the data of Nu_x gotten in this study with data realized from published studies when $N\,t$ and $N\,b$ take different values and $\xi \to \infty$ with other limiting conditions. As recorded in Tables 2, the comparisons showed that the current study strongly correlate with the existing studies.

Table 1: Computational values of Nu_x in comparison with published works for varying values of Nt and Nb

	Dalir (2015)	Khan & Pop (2010)	Present	Dalir (2015)	Khan & Pop (2010)	Current	Dalir (2015)
Nt	Nb = 0:1			Nb = 0:3			
0:1	0.95238	0.9524	0.95238	0.25213	0.2522	0.25216	0.05422
0:3	0.52008	0.5201	0.52008	0.13549	0.1255	0.13551	0.02912
0:5	0.32105	0.3210	0.32106	0.08328	0.0833	0.08330	0.01799

4. Analysis and discussion of results

It is noteworthy that figures 2-19 have been included in this section to elucidate the reactions of the emerging parameters on the profiles of velocity, temperature, concentration field including the skin frictional factor and the Nusselt number which correspond to heat transfer mechanism. The pattern of the velocity profile for variations in α and δ is demonstrated in figure 2. It is noted that a rise in α causes a shrink in the momentum boundary layer and as well decelerates the velocity profile due a decrease in the retardation time. However, figure 2 also demonstrate that an accelerating flow occurs with higher magnitudes of δ. This trend is induced due to the direct variation that exist between the stretching rate a and the Deborah number δ. Such a relationship elevates the momentum boundary structure and as such, the Jeffrey nanofluid movement is raised. These observations coincide with that of Dalir et al. (2015). The magnetic field impact on the fluid speed is depicted in figure 3. Clearly, a decelerated flow occurs with a rise in M due to the generation of Lorentz force. The Lorentz force is induced by the interaction that takes place between the transverse magnetic field and the electro-conducting Jefferey nanofluid. Thus, higher M causes a stronger resistance to the fluid movement fluid as shown in this figure. The absence of the magnetic field $M = 0$ propels a higher velocity profile as illustrated in this figure. In this view, magnetic field can be imposed to measure the movement of the fluid.

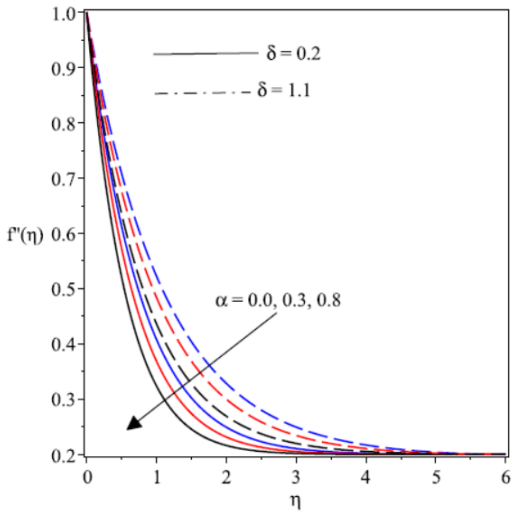

Fig. 2 Velocity profiles for variation in α

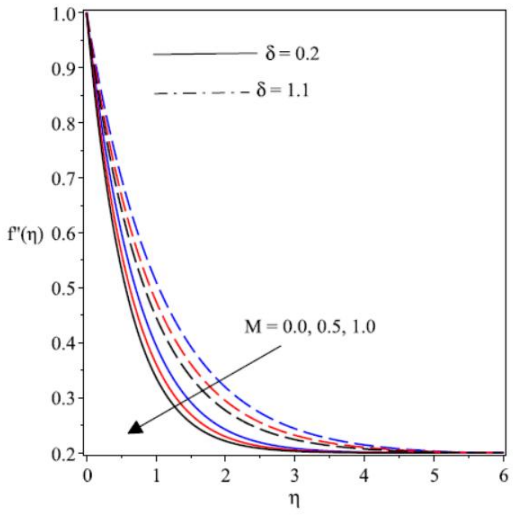

Fig. 3 Velocity profiles for variation in M

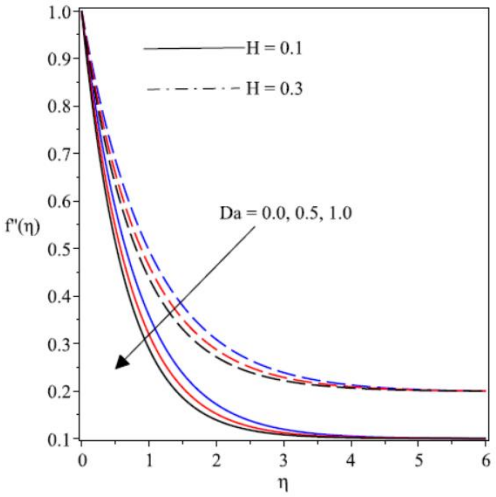

Fig. 4 Velocity profiles for variation in α

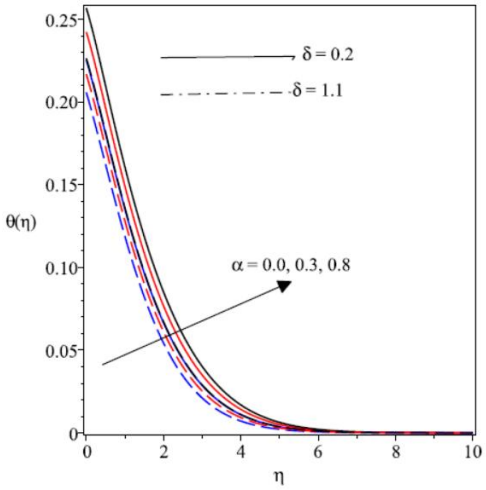

Fig. 5 Velocity profiles for variation in M

Figure 4 features the velocity distribution versus the stream distance η for escalating values of the Darcy number Da in the presence of the stretching term H. A shrunk hydrodynamic boundary film and velocity profiles is exposed by higher values of Da whereas an opposite trend manifests as H rises in strength. The Darcy number represents the porosity term in which there is a resistance to fluid motion by the increase in Da but the Jeffrey nanoliquid motion significantly accelerates when the stretching term H augments. The implication of the effect of α and δ on the heat distribution and nanoparticles volume concentration is exemplified in figure 5 and 6. There is an improvement in the temperature distribution and nanoparticles volume concentration by higher magnitude of α whereas the thermal/concentration field depletes with an increase in the Deborah number δ. This fact is in view of the escalating nature of the relaxation time but a fall in the retardation time due to higher α. Thus, higher magnitude of α corresponds to the dominance of relaxation time over that of retardation time and such a trend leads to the enhancement of thermal/concentration field. Meanwhile, a fall in the temperature/concentration profiles due to δ is explained by the direct relationship that exist between the relaxation time and δ. In view of this, higher relaxation time resulted from larger δ and consequently, there is a thin heat boundary layer and low temperature distribution.

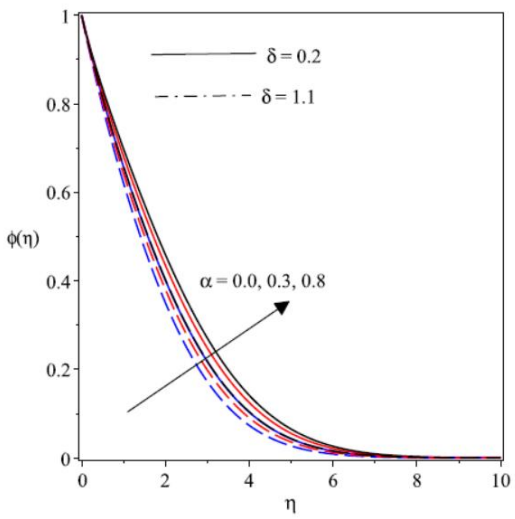

Fig. 6 Concentration profiles for α

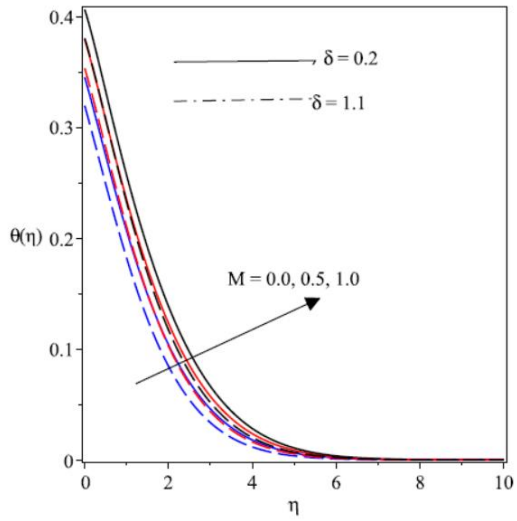

Fig. 7 Temperature profiles for M

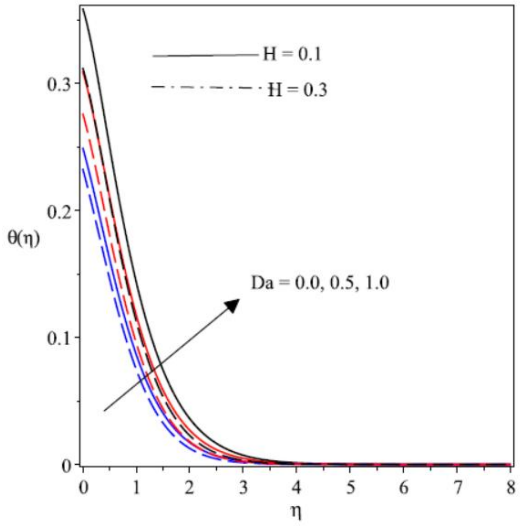

Fig. 8 Temperature profiles for varying *Da*

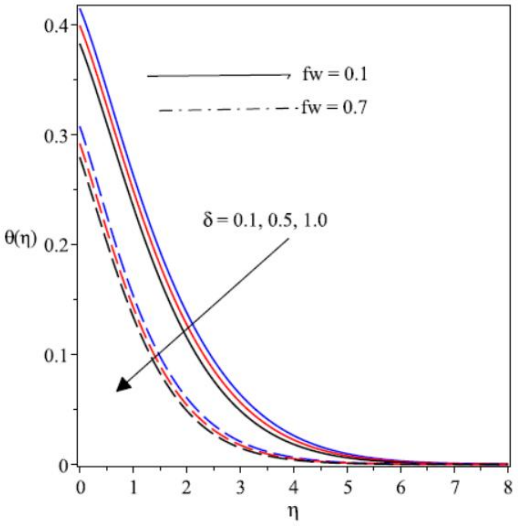

Fig. 9 Temperature profiles for varying δ

Figure 7 portrays the reaction of M on the non-dimensional temperature distribution $\theta(\eta)$. There is uplifting in the thermal regime by a rise in M owing to flow resistance caused by the Lorentz force. The resistance to the fluid movement due to this force induces a rise in the fluid friction which leads to generation of additional heat and thus the Jeffrey nanoliquid temperature advances. Likewise, escalating values of Da causes the heat distribution to soar as exemplified in figure 8 whereas the the thermal field dampen when the stretching term H is present. In the meantime, suction term fw creates a thin heat boundary film structure and deplete temperature profile as found in figure 9. The impact of $N\,t$ in the presence of the $N\,b$ is illustrated in Figure 10. Both parameters strengthen the thermal field and induce a higher surface temperature. As found in the energy equation (8), both $N\,t$ and $N\,b$ vary directly to the dimensionless temperature $\theta(\eta)$ and as such, a rise in $N\,t$ and $N\,b$ corresponds to improving temperature of the Jeffrey nanoliquid. Furthermore, figure 11 explains the reaction of $T\,r$ on the thermal region with variation in ξ is present. An increase in both quantities uplift the heat layer plus temperature profile. Higher values of ξ indicates a lower heat transfer resistance at the sheet surface as compared to that of the internal resistance, thereby there is a boost in the heat distribution when ξ increases.

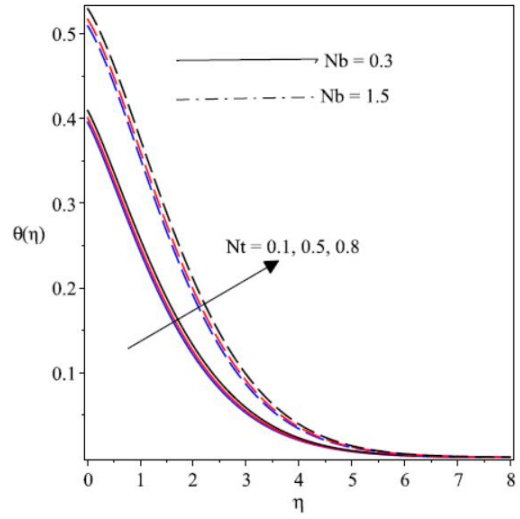

Fig. 10 Graph of temperature for $N\,t$

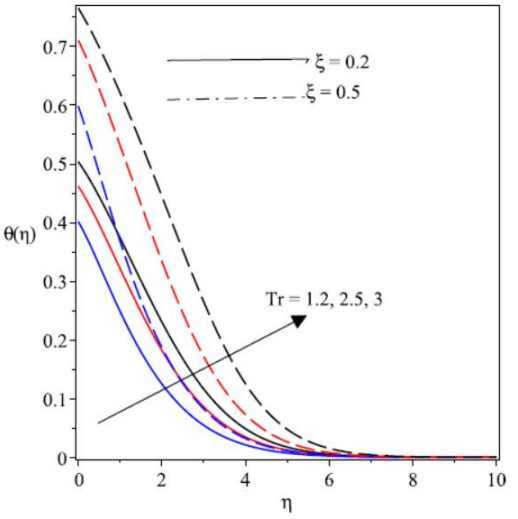

Fig. 11 Profile of temperature varying $T\,r$

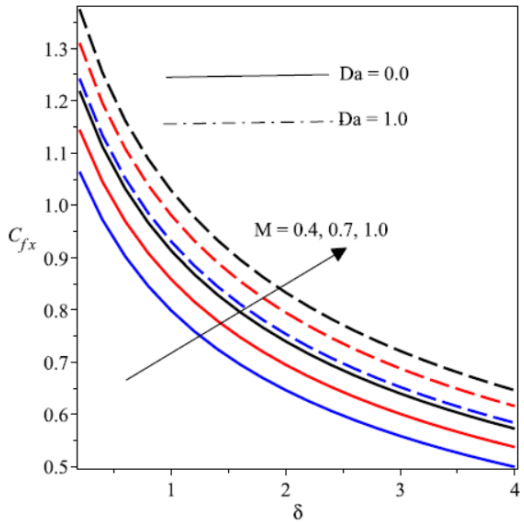

Fig. 12 Plot of C_{fx} for varying M & Da

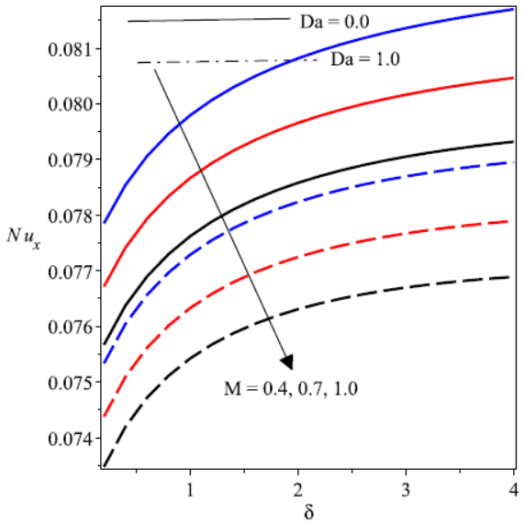

Fig. 13 Graph of Nu_x for values of M & Da

Figures 12 and 13 respectively portray the reaction of C_{fx} and Nu_x for the combined effects of M and δ in the presence/absence of Darcy number Da. Observation reveals that C_{fx} is an increasing function of M and Da. The resistance offered to the motion of the Jeffrey nanoliquid by the Lorentz force raises the surface drag force as M increases. However, a rise in δ lowers C_{fx} as found in figure 12. This is based on the fact that growing values of δ corresponds to low viscosity of the fluid whereas the Jeffrey fluid elasticity is enhanced and as such, there reduction in C_{fx}. The exact opposite of the trends in figure 12 are found for the heat transfer mechanism Nu_x in figure 13. Higher heat transfer across the sheet surface can be derived by increasing the magnitudes of δ and in the absence of Da. Figure 14, 15 and 16 clearly reveal that the quantity of the heat transfer Nu_x diminishes with higher magnitudes of $N\,b$, $N\,t$ and Ec whereas with a rise in $P\,r$ as well as ξ, Nu_x significantly appreciates. Figure 17 depicts the impact of α and H on C_{fx}. A growth is found in C_{fx} by a rise α but the converse occurs for a rise in H. A rising pattern of C_{fx} due to α connotes that the Jeffrey nanofluid particles requires additional time to stabilize to a stable state and in this view the surface drag force improves. Conversely, there is a significant rise in Nu_x by boosting the values of H while heat transfer is impeded by a rise in α as portrayed in figure 18. Figure 19 portrays the behaviour of $N\,t$ on the nanoparticles concentration profile with variation of $N\,b$. A rise in $N\,t$ augments concentration profiles whereas a depletion concentration profile is found by higher magnitudes of $N\,b$.

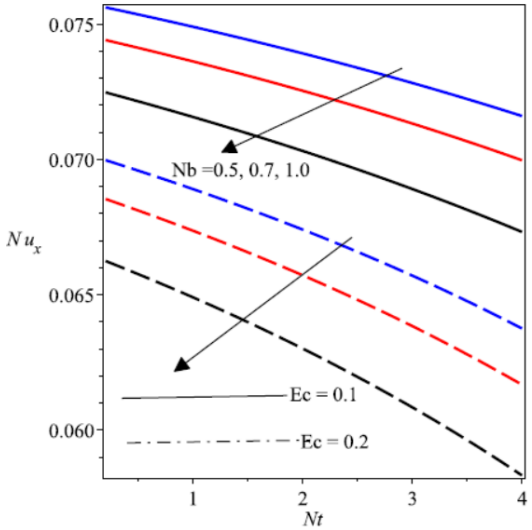

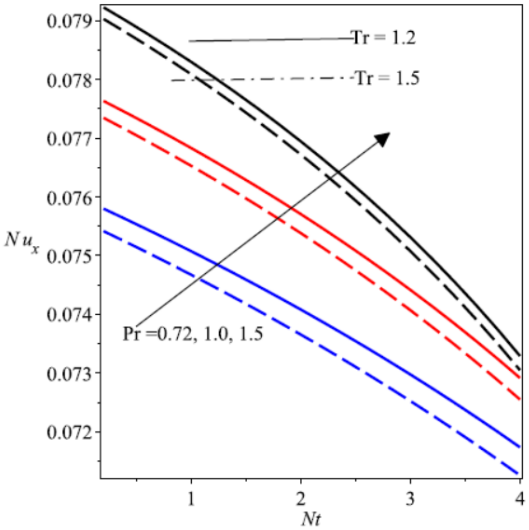

Fig. 14 Plot of Nu_x for varying $N\,b$ &Ec Fig. 15 Graph of Nu_x for varying $P\,r$ &$T\,r$

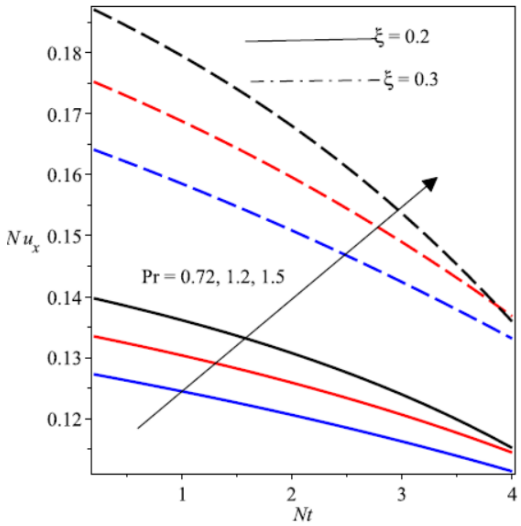

Fig. 16 Profiles of Nu_x for various $P\,r$ & ξ

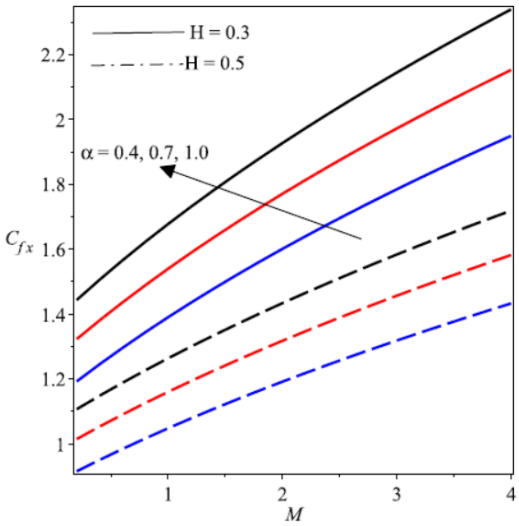

Fig. 17 Plot of C_{fx} for variation in H & α

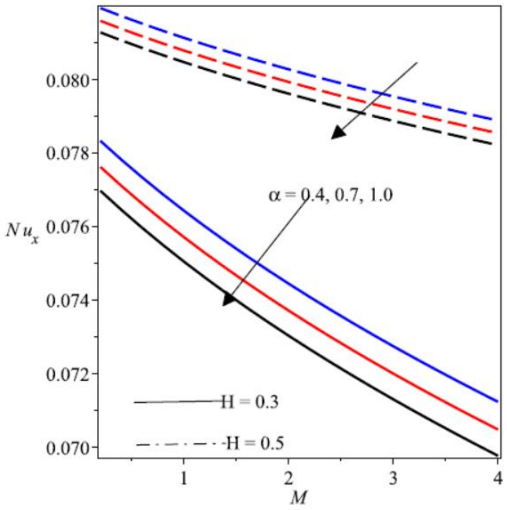

Fig. 18 Plot of Nu_x for variation in α & H

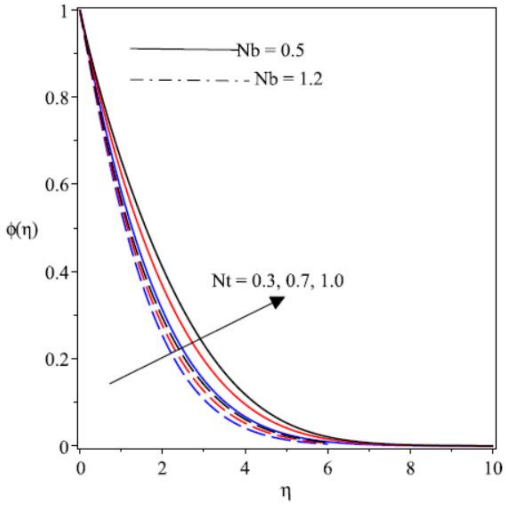

Fig. 19 Concentration profiles for Varying $N\,t$

5. Conclusion

The dynamics of heat transfer mechanism in stagnation-point flow of hydromagnetic Jeffery nanoliquid along a convectively heated porous expanding sheet is investigated in this study. The formulated mathematical model features nonlinear thermal radiation, viscous dissipation together with ther mophoresis and Brownian motion effects. The remodelling of the main equations from partial to ordinary derivatives are carried out by means of suitable similarity quantities and subsequently solved numerically by employing shooting technique in conjunction with Runge-Kutta Fehlberg scheme. The consequence of the analysis compared favourably with existing studies under limiting conditions while various graphs are constructed to demonstrate the trend of the emerging physical terms on the transport regions. Conclusively, the study reveals that:

- Heat transfer appreciates when the surface convection term ξ, Prandtl number $P\,r$, stretching term H and Deborah number δ improve in magnitude whereas the converse trend occurs with when Eckert number Ec, thermophoresis term $N\,t$, magnetic field term M and Brownian motion term $N\,b$ escalates.
- Surface frictional drag C_{fx} depreciates for higher values of Deborah number δ and stretching term H but an escalating nature of C_{fx} is found when the Darcy number Da and magnetic field parameter M escalates in magnitude.
- An appreciating surface temperature is found with higher magnitudes of the magnetic field, thermophoresis, Brownian motion, temperature ratio parameters whereas such a

trend is reversed with advancing nature of the Deborah number and suction parameters *fw*.

- A decelerating motion of the Jeffrey nanoliquid is found when the magnetic field and Darcy parameters rises but a higher velocity profile occurs with a rise in δ and H as the thermophoresis quantity $N\ t$ promotes a rise in the concentration profile.

References

[1]. Akinbobola, T. E. and Okoya, S. S. (2015). The flow of second grade fluid over a stretching sheet with variable thermal conductivity and viscosity in the presence of heat source/sink, *Journal of Nigeria Mathematical Society* 34: 331-342.

[2]. Alshomrani, A. S., Ullah, M. Z., Capizzano, S. S., Khan, W. A. & Khan, M. (2018). Interpretation of Chemical reactions and activation energy for unsteady 3D flow of Eyring-Powell magneto nanofluid, *Arabian Journal for Science and Engineering* 2018: 1-11. doi.org/10.1007/s13369- 018-3485-7

[3]. Anderson, H. I. (2002). Slip flow past a stretching surface, *Acta Mechanica* 158: 121-125.

[4]. Basha, H. T., Gunakala, S. R., Makinde, O. D. & Sivaraj, R. (2018). Chemically reacting unsteady flow of nanofluid over a Cone and Plate with activation energy, *Defect and Diffusion Forum* 387: 343-351.

[5]. Batool, K. & Ashraf, M. (2013). Stagnation Point flow and heat transfer of a magneto-micropolar fluid towards a shrinking sheet with mass transfer and chemical reaction, *Journal of Mechanics* 29: 411-422.

[6]. Bhattacharyya, K. MHD Stagnation-Point Flow of Casson Fluid and Heat Transfer over a Stretch ing Sheet with Thermal Radiation, Journal of 5ermodynamics, 2013, 1-9 (2013).

[7]. Choi, S. U. S. & Eastman J. A. (1995). Enhancing thermal conductivity of fluids with nanoparti cles, in: Enhancing Thermal Conductivity of Fluids with Nanoparticles, 99-105 (1995).

[8]. Crane, L. J. (1970). Flow past a stretching plate. *Communicatios Breves* 21: 645-647.

[9]. Dalir, N., Dehsara, M. & Nourazar, S. S. (2015). Entropy analysis for magnetohydrodynamic flow and heat transfer of a Jeffrey nanofluid over a stretching sheet, *Energy* 79: 351-362.

[10]. Fatunmbi, E. O. & Adeniyan, A. (2018). Heat and mass transfer in MHD micropolar fluid flow over a stretching sheet with velocity and thermal slip conditions, *Open Journal of Fluid Dynamics* 8: 195-215.

[11]. Fatunmbi, E.O & Fenuga, O. J. (2017). MHD micropolar fluid flow over a permeable stretching sheet in the presence of variable viscosity and thermal conductivity with Soret and Dufour effects, *International Journal of Mathematical Analysis and Optimization: Theory and Appli cations* 2017: 1-17.

[12]. Fatunmbi, E. O. & Adeniyan, A. (2018). MHD stagnation point-flow of micropolar fluids past a permeable stretching plate in porous media with thermal radiation, chemical reaction and viscous Dissipation, *Journal of Advances in Mathematics and Computer Science* 26(1): 1-19.

[13]. Fatunmbi, E. O. & Okoya, S. S. (2020). Heat transfer in boundary layer magneto-micropolar fluids with temperature-dependent material properties over a stretching sheet, *Advances in Materials Science and Engineering*, 2020, 1-11 (2020).

[14]. Gbadeyan, J. A., Titiloye, E. O. & Adeosun, A. T. (2020). Effect of variable thermal conductivity and viscosity on Casson nanofluid flow with convective heating and velocity slip, *Heliyon* 6: 1-10.

[15]. Hayat, T, Shehzad, S. A., Qasim, M. & Obaidat, S. (2012). Radiative flow of Jeffery fluid in a porous medium with power law heat flux and heat source, *Nuclear Engineering and Design* 243, 1-5.

[16]. Hiemenz, K. Die Grenzschicht an einem in den gleich for mingen flussigkeits strom eigetauchten graden Kreiszylinder, *Dingerls Polytech. J.* 326: 321-324.

[17]. Hosseinzadeh, K, Gholinia, H, Jafari, B, Ghanbarpour, A., Olfian, H & Ganji, D. D. (2018). Non linear thermal radiation and chemical reaction effects on Maxwell fluid flow with convectively heated plate in a porous medium, *Wiley*, 45: 1-11.

[18]. Hsiao, K. (2017). Micropolar nanofluid flow with MHD and viscous dissipation effects towards a stretching sheet with multimedia feature. *International Journal of Heat and Mass Transfer* 112: 983-9?90.

[19]. Ibrahim, W., Shankar, B., Nandeppanavar, M. M. (2013). MHD stagnation point flow and heat transfer due to nanofluid towards a stretching sheet, *International Journal of Heat and Mass Transfer* 56: 19.

[20]. Ibrahim, W. & Gamachu, D. (2016). Nonlinear convection flow of Williamson nanofluid past a radially stretching surface, *AIP Advances* 9: 1-13.

[21]. Iqbal, Z., Azhar, E., Mehmood, Z., Maraj, E. N. (2017). Melting heat transport of nanofluidic problem over a Riga plate with erratic thickness: Use of Keller Box scheme, *Results in Physics* 7: 36483658

[22]. Ishak, A., Jafar, K. Nazar, R., and Pop I. MHD Stagnation point flow towards a stretching sheet, *Physica A* 388: 3337-3383.

[23]. Jena, S., Mishra, S. R. and Dash, G. C. (2016). Chemical Reaction Effect on MHD Jeffery Fluid Flow over a Stretching Sheet Through Porous Media with Heat Generation/Absorption, *Int. J. Appl. Comput.*: 1-14.

[24]. Kasim, A. R. M., Arifin, N. S., Zokri, S. M. & Salleh, M. Z. (2019). Fluid-Particle Interaction with Buoyancy Forces on Jeffrey fluid with Newtonian Heating, *CFD Letters* 11(1): 1-16.

[25]. Khan, W. A. & Pop, I. (2010). Boundary-layer flow of a nanofluid past a stretching sheet, *Int J Heat Mass Tran* 53: 2477e83.

[26]. Kumar, R. V. M. S. S. K., Kumar, G. V., Raju, C. S. K., Shehzad, S. A. & Varma, S. V. K.J. (2018). Analysis of Arrhenius activation energy in magnetohydrodynamic Carreau fluid flow through improved theory of heat diffusion and binary chemical reaction, *Phys. Commun.* 2: 1-15.

[27]. Kumar, L. (2009). Finite element analysis of combined heat and mass transfer in hydromagnetic micropolar flow along a stretching sheet, *Comput Mater Sci* 46: 841-848.

[28]. Lakshmi, R. V., Sarojamma, G., Sreelakshmi, K & Vajravelu. (2019). Transfer Analysis in a micropolar fluid with nonlinear thermal radiation and second-order velocity slip. *Applied Mathematics and Scientific Computing* 30: 385-395.

[29]. Mabood, F. & Das, K. (2019). Outlining the impact of melting on MHD Casson fluid flow past a stretching sheet in a porous medium with radiation, *Heliyon* 5: e01216.doi: 10.1016/j.heliyon.2019.e01216.

[30]. Mabood, F., Ibrahim, S M. & Khan. W. A. (2019). Effect of melting and heat generation/absorption on Sisko nanofluid over a stretching surface with nonlinear radiation. *Physica Scripta* 94(6): 065701.

[31]. Mabood, F., Imtiaz, M, Alsaedi, A. & Hayat, T. (2016). Unsteady Convective Boundary Layer Flow of Maxwell Fluid with Nonlinear Thermal Radiation: A Numerical Study, *IJNSNS* 17(5): 221-229.

[32]. Makinde, O. D. & Animasaun, I. L.. (2016). Bioconvection in MHD nanofluid flow with nonlinear thermal radiation and quartic autocatalysis chemical reaction past an upper surface of a paraboloid of revolution, *International Journal of Thermal Sciences* 109: 159-171.

[33]. Mishra, R. (2017). Slip effect on HMHD flow and heat transfer of Jeffrey nanofluid over a stretching sheet in the presence of nonlinear thermal radiation and chemical reaction, *International Journal of Engineering Sciences — Research Technology* 6(4): 1-17.

[34]. Pal, D., Mondal, S. & Mondal, H. (2019). Entropy generation on MHD Jeffrey nanofluid over a stretching sheet with nonlinear thermal radiation using spectral quasilinearisation method, *International Journal of Ambient Energy* DOI: 10.1080/01430750.2019.1614984

[35]. Nadeem, S., Haq, R.U. & Khan, Z. H. (2014). Numerical solution of non-Newtonian nanofluid flow over a stretching sheet, *Appl Nanosci* 4: 625e31.

[36]. Nadeem, S., Zaheer, S. and Fang, T. (2011). Effects of thermal radiation on the boundary layer flow of a Jeffrey fluid over an exponentially stretching surface, *Numer Algor* 57: 187?05.

[37]. Prasannakumara, B. C., Gireesha, B. J., Krishnamurthy, M. R. & Kumar, K. G. (2017). MHD flow and nonlinear radiative heat transfer of Sisko nanofluid over a nonlinear stretching sheet, *Informatics in Medicine Unlocked* 9: 123-132.

[38]. Ramesh, K. (2018). Effects of viscous dissipation and Joule heating on the Couette and Poiseuille flows of a Jeffrey fluid with slip boundary conditions, *Propulsion and Power Research* 7(4):329- 341

[39]. Ramzan, M, Ullah, N., Chung, J. D., Lu, D. & Farooq, U. (2018). Buoyancy effects on the radiative magneto Micropolar nanofluid flow with double stratification, activation energy and binary chemical reaction, *Scientific Reports* 7: 1-15.

[40]. Salem, A. M. & Fathy, R. (2012). Effects of variable properties on MHD heat and mass transfer flow near a stagnation point towards a stretching sheet in a porous medium with thermal radiation, *Chin. Phys. B* 21(5): 1-12.

[41]. Shateyi, S. & Marewo, G. T. (2018). Numerical solution of mixed convection flow of an MHD Jeffery fluid over an exponentially stretching sheet in the presence of thermal radiation and chemical reaction, *Open Phys.* 16: 249-259.

[42]. Zeeshan, A. & Majeed, A. (2016). Heat transfer analysis of Jeffery fluid flow over a stretch ing sheet with suction/injection and magnetic dipole effect, *Alexandria Eng. J* 55(3): 1-11. doi.org/10.1016/j.aej.2016.06.014

